JOURNAL OF PROPULSION AND POWER
Vol. 19, No. 6, November–December 2003

Combustion of Solid-Fuel Slabs Containing Boron Particles in Step Combustor

Helmut K. Ciezki,* Joachim Sender,† Walter Clauß,‡ Albert Feinauer,§ and Albert Thumann¶
DLR, German Aerospace Center, D-74239 Hardthausen, Germany

The combustion processes of solid-fuel slabs with and without boron-particle addition have been investigated in a planar rearward-facing step combustor. The study was performed under conditions of air inlet velocity and temperature relevant to ramjet applications. The highly turbulent, multiphase combustion process has been analyzed with various intrusive and nonintrusive diagnostic techniques. Gas-phase temperature distributions and particle velocities as well as concentrations of various stable reaction products have been determined in order to show the movement and the combustion of the reacting particle phase in the recirculation zone and the downstream boundary layer with the embedded reaction zone. Large-scale, coherent vortex structures have been observed. These structures exist predominantly in the region above the hydrocarbon diffusion flame located inside the developing boundary layer and show an intense and highly turbulent mixing process. The results show dependencies of the energy release on the flowfield related to the presence of reacting or nonreacting particles.

Nomenclature

B	=	combustor width, mm
$D_{3,2}$	=	Sauter mean diameter, μm
d	=	particle diameter, μm
$\dot{g}_{\text{air}}$	=	air mass flux, kg/m^{2}s
H	=	step height, mm
h	=	combustor height, mm
L_R	=	length of primary recirculation zone, mm
$\dot{m}_{\text{air}}$	=	air mass-flow rate, kg/s
Re_H	=	Reynolds number based on step height H
St_P	=	particle Stokes number
T	=	gas-phase temperature, K
T_{air}	=	air temperature at combustor inlet, K
t	=	time, s
U	=	velocity component in x direction, m/s
U_{CH4}	=	methane feeding velocity of data from Ref. 26, m/s
U_0	=	air intake velocity above step, m/s
u'	=	rms value of U
V	=	velocity component in y direction, m/s
v'	=	rms value of V
w	=	trace of the outer border of the outer zone, mm
X_i	=	volume flow ratio of species i
x	=	Cartesian coordinate (streamwise direction; see Fig. 1b), mm
Y_i	=	mass flow ratio of species i
y	=	Cartesian coordinate (transverse direction; see Fig. 1b), mm
z	=	Cartesian coordinate (spanwise direction, see Fig. 1b), mm
β	=	inclination angle
ΔL	=	horizontal distance of vortices, mm
ϕ	=	equivalence ratio

Subscripts

air	=	airflow, conditions at the inlet
f	=	fuel
g	=	gas phase
H	=	at step, related to step height H
p	=	particle phase

I. Introduction

SOLID fuels are of interest for airbreathing propulsion systems such as ramjets and ducted rockets because they are relatively easy to handle. The addition of combustible particles like aluminum or boron to the commonly used hydrocarbon-type binders offers the possibility of building more compact engines. Because of its theoretically highest energy release per unit volume, boron is of special interest for the development of volume-reduced engines or engines with better flight performances.[1,2]

Unfortunately, in real ramjet engines and also in model combustors the formation of condensed oxides on the surfaces of the boron particles prevents a complete boron consumption. This behavior is mainly caused by the significantly lower melting and boiling points of boron-oxide B_2O_3 melting point (MP): 723 K, boiling point (BP): 2316 K, Ref. 3) in comparison to pure boron (MP: 2350 K, BP: 4138 K, Ref. 3), in combination with the surface tension behavior of molten B_2O_3 (e.g., see Ref. 4). The boron oxide forms thin liquid layers covering each boron particle immediately after ignition when the ambient temperatures are significantly below the B_2O_3 boiling point. These layers act as barriers between the particle surface and the oxygen in the surrounding gas phase and thus reduce the rate of chemical reaction. This hinders a quick and efficient combustion process, given the low residence time of the boron particles inside real engines. The second ignition stage, which leads to a sustained combustion process of the boron particles, occurs only under certain conditions at higher surrounding gas temperatures exceeding 1900 K. This has been reported by various authors, for example, Ref. 5, based on the investigation of the ignition and combustion behavior of boron particles in a flat-flame burner device by Macek.[6] Detailed one-dimensional calculations of the reignition behavior have been performed by various authors. Also the rupture behavior of the B_2O_3 layer has been analyzed by Meinköhn.[4] Through this study the derivative of the surface tension with respect to the temperature $\partial\sigma/\partial T$ has been identified as an important parameter, in addition to the heat flux.

Basic investigations on single boron particles as well as on particle cloud ignition and combustion phenomena have been conducted in the past in different experimental devices such as burners, shock tubes, and closed vessels (e.g., see Refs. 7–14). With these and

Received 9 August 2000; revision received 10 December 2002; accepted for publication 17 March 2003.

*Head Ramjet Propulsion and Chem.-Phys. Laboratories, DLR, Space Propulsion Institute Lampoldshausen, D-74239 Hardthausen, Germany; helmut.ciezki@dlr.de. Member AIAA.
†Head Combustion Chamber Technology, Space Propulsion Institute.
‡Project Scientist, DLR, Space Propulsion Institute.
§Project Engineer, DLR, Space Propulsion Institute.
¶Project Scientist, DLR, Space Propulsion Institute.

other data ignition and combustion models have been developed for numerical simulations. More recent publications present investigations on the influence of additives or particle coatings for improved boron-particle ignition and combustion, (e.g., Refs. 12 and 15).

Apart from these studies the complex multiphase flow and combustion processes in a real solid-fuel ramjet combustor are not completely understood at present, although important efforts have been made in the last decades. To obtain a better understanding of the governing processes of combustion and the respective flowfield, processes like the movement of single particles and their ignition within the flowfield and the flame-holding behavior have been investigated separately. Sudden expansions behind backward or rearward-facing steps, bluff-body-type flame holders, etc. are often used for flame stabilization in ramjet combustors. Basic investigations of nonreacting two- or three-dimensional dump-type combustor flows, to which backward or rearward-facing step flows and sudden expansion flows belong, have been conducted extensively in the past. A review of investigations up to 1981 on turbulent flow reattachment is given by Eaton and Johnston.[16] In more recent investigations laser-based diagnostics have often been used, giving further insight into the processes (e.g., Refs. 17–19).

Most of the reacting flows investigated using rearward-facing step devices were premixed systems, where air and fuel have been mixed before entering the area behind the step (see Refs. 20–24). Less common are the basic investigations on the flowfield and combustion processes in nonpremixed systems in sudden expansion flows, especially with regard to solid-fuel combustion. Schadow et al.,[25] for example, conducted temperature and concentration measurements in a tubular combustor. Krametz and Schulte[26] investigated the flame-stabilization process in a planar, rearward-facing step combustor, feeding methane through a porous bottom plate behind the step in order to simulate a gasifying solid-fuel surface. Numerical calculations of the flowfield and combustion process in a rearward-facing step combustor have been performed by Tsau and Strahle[27] in which hydrogen and methane were fed through a distinct area in the combustor bottom. Metallized solid fuels have been investigated for example, by Gany and Netzer,[28] who observed the movement and the combustion of boron particles in a reacting boundary layer above a solid fuel surface in various experimental devices. Numerical calculations of the movement of single boron particles and their ignition and combustion have been conducted for example by Jarymowycz et al.[29] for small particle sizes in a high-velocity environment ($Ma > 0.8$) and also by Natan and Gany[30] for larger particle diameters ($d > 25\ \mu$m) and low Mach numbers ($Ma < 0.1$).

The investigation presented here provides new insight into the flowfield and combustion processes of solid fuels with embedded boron particles of small diameter ($D_{32} = 0.96\ \mu$m) under conditions of air inlet velocity and temperature relevant to ramjet applications. A planar rearward-facing step combustor was used as a basic experimental setup. The combustor is equipped with window segments on both sides of the chamber with an N_2-protection flow enabling direct access for optical and especially laser-based diagnostic tools to the reacting multiphase flow field immediately above the solid-fuel slabs. The chamber pressure was about 1 bar so that (laser) diagnostic tools could be operated farther away from optically dense conditions to facilitate observation. In these experiments special attention was given to the region of the recirculation zone and the region downstream immediately, containing the developing reacting subboundary layer.

The present publication is based on a paper presented at the 36th AIAA Joint Propulsion Conference in 2000 in Huntsville, Alabama.[31] The data presented in the present paper were further evaluated in greater detail and recent results were added.

II. Experimental Apparatus

A. Test Facility

A sketch of the step combustor test facility is presented in Fig. 1. The test section has a rectangular cross section of 150 mm width and 45 mm height. This facility was originally used by Krametz and Schulte[26] and has been significantly modified for the investigation presented here. The solid-fuel slabs of 200 mm in length and

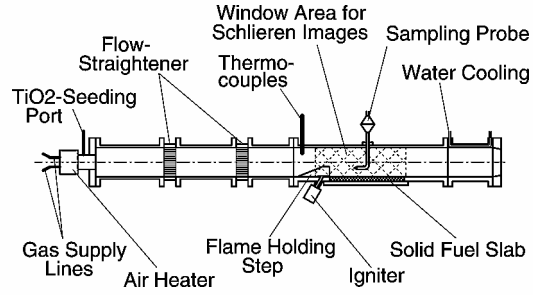

Fig. 1a Sketch of the test facility with the planar step combustor and sampling probe.

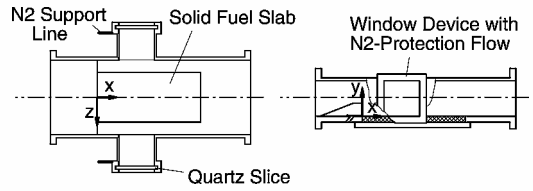

Fig. 1b Top view (left) and side view (right) of the combustor section with window segments for laser-optical diagnostics.

100 mm in width were mounted flush to the bottom of the combustion chamber directly behind the 20 mm high rearward-facing step. Pollution of the windows by particles, soot, and combustion residues is reduced by a clearance of 25 mm between the side walls and the solid-fuel slab. For laser-based diagnostic tools additional window segments with quartz slices at the end of rectangular tubes have been used, as can be seen in Fig. 1b. Necessary pollution reduction has been realized by a slight flow of nitrogen (~3% of the air mass flow at the combustor inlet) through these tubes. The inner height of the rectangular window tubes is the same as the inner height of the combustor (45 mm) so that direct access to the combustion process directly above the solid-fuel plate is possible. These window segments can be placed at various positions along the combustor in order to allow measurements at a range of precise combustion chamber cross sections behind the flame-holding step. For the color schlieren images large quartz slices, which are longer than the solid-fuel slabs, were used as windows on both sides of the combustor.

Vitiated hot air, which is produced by heating the airflow with an H_2-O_2 burner and replenishment of oxygen, is made homogeneous by two flow straighteners and sieves before entering the combustor. No nozzle was attached to the exit of the combustion chamber. Thus, nearly ambient pressure was maintained inside. The temperature of the heated airflow was monitored by two thermocouples positioned in a cross section immediately before the flame-holding step. The mass-flow rates were determined with sonic orifices. The coordinate origin is set in the lower corner of the rearward-facing step at the center plane (in the middle of the chamber width), as can be seen in Fig. 1b.

B. Diagnostic Setup

Color Schlieren

Schlieren techniques offer the possibility to visualize refractive index gradients in flowfields and combustion processes. Most of the black-and-white or monochromatic schlieren methods present the different gradient values as different shades of gray. In strongly particle-laden flows, however, an intensity reduction is also caused by scattering and absorption by the particles. Consequently, the interpretation of black-and-white or monochromatic schlieren images under these conditions is much more difficult and should be done carefully. Color schlieren methods, however, based on the dissection technique[32] offer the possibility to obtain results in environments nearer to optically dense conditions. As can be seen in the sketch in Fig. 2, the color filter source mask is positioned in the focal plane of the first schlieren mirror. Illuminated by a light source, the color mask produces light beams with different colors, which represent different deflection angles and thereby different refractive index

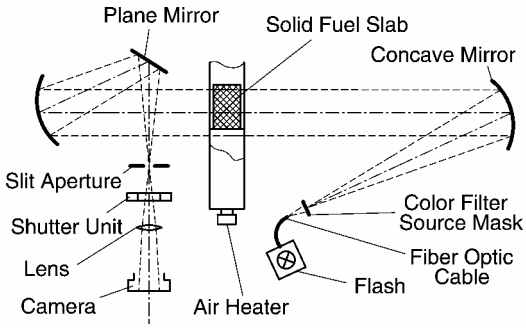

Fig. 2 Sketch of the color schlieren setup at the planar step combustor test facility.

gradients. While these light beams transit the particle-containing investigation area, their intensity is lowered, but the different colors are not changed. Thus, in a first approximation the color schlieren image gives important information about the (macroscopic-averaged) refractive index gradient distribution of the gas phase.

Figure 2 presents a sketch of the color schlieren apparatus in the typical Z-setup. A plane mirror has been added on the image side because of the limited space in the test cell. A modified Drello Xenon flash light with a flash duration of 13 μs has been used as light source. A shutter unit with exposure times significantly lower than 1 μs has been positioned in front of the Hasselblad EL 500 camera in order to reduce the contribution of the superimposed strong thermal emissions from the combustion process on the schlieren images.

The location of the color segments on the color filter mask has been chosen to be similar to that of a rainbow so that there is a clear relation between the refractive index gradient and the color. This kind of color coding has been described in detail in Ref. 33. The schlieren apparatus is adjusted in such a way that the green color represents refractive index gradients near to zero. Detailed information about this technique and also the theoretical background is given in Refs. 33–35.

Mie-Scattering and Particle Image Velocimetry

Particle image velocimetry (PIV) is a nonintrusive two-dimensional flow-visualization technique whereby tracer particles are commonly added to the flow to determine qualitative as well as quantitative information[36–38] about the flowfield. The aim of the investigation presented here was the visualization of the movement of the reacting particle phase, which is ejected from the solid-fuel slabs, so that no further particles were added to the airflow.

A light sheet is formed from the laser beams of a transportable laser system and is introduced in the center plane at $z = 0$ through an additional window at the top of the combustor. The scattered light from the double-illuminated particles is observed and collected by a charge-coupled device camera through one of the window segments with a protection flow at the side wall. The double illumination of the particles was achieved by means of an adjustable delay between two laser pulses. The results discussed in this publication were achieved with the cross-correlation technique. Therefore the scattered light from two consecutive laser pulses was recorded on two separate images, and the movement of the particles was tracked from their shift between the two images obtained (e.g., for more details see Refs. 39–42).

Laser Doppler Velocimeter

A two-dimensional laser Doppler velocimeter (LDV) from Dantec, equipped with a 5-W argon ion laser (Innova 90, Coherent), and two burst spectrum analyzers (BSA, Dantec) were used to measure the velocities using forward scatter sampling. The focal length of the transmitting lens was 300 mm. The conversion factor for this configuration was 8.67 ms^{-1}/MHz for 488 nm. The beam pairs were rotated at 45 deg along the z axis to improve resolution for both x and y velocity components. A total of 6100 samples was taken at each measurement point, scanning the incoming LDV signal at 5 Hz. Data reduction was performed using standard software.

For the determination of the velocity distributions at each cross section, the LDV was mounted on a three-dimensional-traversing unit, which was controlled by a PC. The velocity profiles were taken vertically starting at the bottom of the combustor in each case to reduce the influence of the surface regression during the combustion process (around 0.06 mm/s for test fuel TF2, i.e., approximately 7 mm for a 2-min test run). Two test runs were made for a complete cross section. Further information is given in Ref. 43.

Coherent Anti-Stokes Raman Spectroscopy

N_2-vibrational coherent anti-Stokes Raman spectroscopy (CARS) is a tool often used for gas temperature measurement, especially when air is used as an oxidizer. In the USED-CARS phase matching geometry laser beams at frequencies ω_1 and ω_2 are "mixed" to generate the coherent laser-like signal at $\omega_3 = 2\omega_1 - \omega_2$. The CARS signal beam could be interpreted as the answer of the investigated molecule to intensive electromagnetic waves through the third-order nonlinear susceptibility. The temperature evaluation is performed via a best-fit method by comparing experimental spectra with a library of theoretical calculated spectra. The accuracy of CARS in clean laboratory environments is typically better than 50 K. The time resolution of the measurements was approximately 8 ns, whereas the spatial resolution of the 0-d measurement volume was below 4 mm in length and 70 μm in diameter.

The CARS system consists of a frequency-doubled Nd:YAG laser and a conventional broadband dye laser as the Stokes laser. The system is transportable in modular units and was situated in a hardened room near the test cell. Only beam-guiding optics, the focussing lens, which was mounted on a movable table for traversing the probe volume to the measuring locations, and the optics for fiber coupling of the signal were located close to the combustion chamber. Further information is given in Refs. 44 and 45.

Sampling Probe System

The modular probe sampling system consists of a water-cooled sampling probe, an exchangeable filter housing that permits a quick filter exchange, a remote control valve unit, a vacuum pump, and exchangeable gas sampling cylinders, as shown in Fig. 3. The sampling probe is mounted in a device at the upper combustor wall, which allows placement of the horizontally oriented tip at any position $y \geq 4$ mm inside the combustor. This device can also be moved to various vertical cross sections.

The sampling probe consists of three thin-walled stainless-steel tubes and an outer copper tube with an outer diameter of 7 mm. The three outer tubes serve to cool the probe with pressurized water. The combustion products are drawn up through a small hole at the tip of the probe and expand into the inner tube with a significantly larger internal diameter of 3 mm. The expansion quench method used here lowers the temperature and thus suppresses further reactions. In multiphase combustion processes care must be taken both with longer cooling times of the particles in comparison to the expanded gas and also with the deposition of particles and condensed reaction

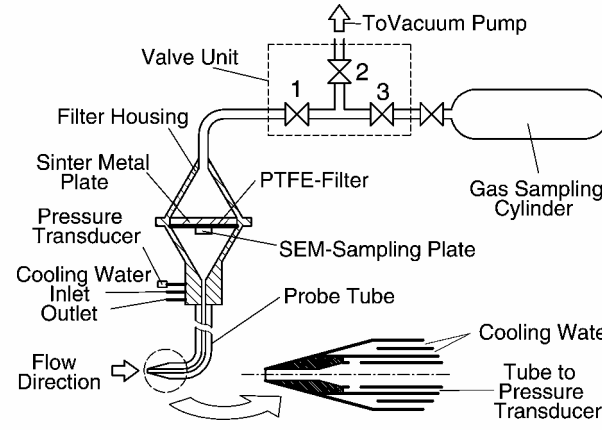

Fig. 3 Schematic of the gas- and particle-sampling probe system.

products on the inner probe tube wall or inside the probe mouth. The second effect can lead to disturbed operating conditions up to a complete blockage and in turn to incorrect results. To monitor the sufficient expansion of the probe gas flow and thereby the correct operation of the probe sampling system, a pressure transducer is connected to the annulus between the inner tubes, as can be seen in Fig. 3. Thus the processes immediately after the widening area in the probe tip can be observed because small holes are drilled into the inner probe tube. The sufficient suppression of further reactions inside the probe has been shown by an earlier test series (Ref. 46). Because of the horizontal orientation of the probe tip and the expansion quench method used for the suppression of further reactions, the sampling procedure is not isokinetic. The results presented here have been obtained at average angles of attack smaller than 15 deg, which have been determined from LDV measurements presented in part 4. The spatial resolution of the sampling probe was estimated in detail in Ref. 35 and is satisfactory under the difficult conditions in the step combustor. A detailed description of the sampling method, particle-following behavior, the quenching procedure, and data evaluation procedure is given also in Refs. 35 and 47.

The sampling procedure starts 10 s after ignition of the solid-fuel slab. Valves 1 and 2 to the vacuum pump are opened to draw up the combustion products through the probe and the filtering assembly. In the filter housing a Teflon-filter with 0.45 μm pore size separates the condensed phase from the gas phase at ambient temperature conditions. Twenty seconds later valve 2 to the vacuum pump is closed, and valve 3 to the previously evacuated sampling cylinder is opened. The pressure in the probe cylinder rises to the pressure prevailing in the combustion chamber within a few seconds. The condensed phase on the filter can be analyzed after the experiment by wet chemistry analysis making use of the Mannitol method for the determination of the boron-oxide content. In this paper all of the (possible) oxide products B_xO_y on the filter are presented as B_2O_3. The gas phase, which has been collected in the gas-sampling cylinder, is analyzed by gas chromatography. Because of the small suction area and the short sampling time, only small probe masses could be obtained, which allowed only the boron-oxide content to be determined.

III. Fuel Composition and Experimental Conditions

The solid-fuel compositions used are based on hydroxyl-terminated polybutadiene (HTPB) as a binder and are listed in Table 1. They are processed from ARCO R 45 M HTPB and isophorone diisocyanate (IPDI) as a curing agent. Test fuel 1 (TF1) has been chosen to show the combustion behavior of a solid fuel without particle additives. Test fuel 2 (TF2) contains 30% boron particles by weight, which are added to the HTPB/IPDI-mixture of test fuel 1. In test fuel 3 (TF3) TiO_2 particles were added with the same mass content to show the influence of the combustible particle phase of TF2 on both the flowfield and the combustion processes in comparison to the noncombustible particle phase.

The amorphous boron particles, manufactured by H. C. Starck, Germany, have an average particle size of 1.75 μm (Sauter size $D_{3,2} = 0.96$ μm) and a purity better than 95%. The size distribution shows that only 10% of the particles have diameters larger than 5 μm and 1% have diameters larger than 10 μm. The titanic-oxide particles, however, delivered from Bayer are much smaller and have a mean diameter of about 0.2 μm.

Table 1 Composition in weight percentage of solid fuels

Test fuel	HTPB	IPDI	B	TiO_2
TF1	91.6	8.4	——	——
TF2	64.1	5.9	30	——
TF3	64.1	5.9	——	30
TF4	87.0	8.0	——	5

The conditions of the three investigated test cases TC1–TC3 are listed in Table 2. Most of the experiments presented here were conducted at TC2 conditions with an air mass-flow rate $\dot{m}_{air}$ at the combustor inlet of about 0.15 kg/s and with a temperature T_{air} of about 800 K. Only a few experiments were conducted with air mass-flows $\dot{m}_{air}$ of 0.11 and 0.19 kg/s, which are described in Table 2 as test cases TC1 and TC3. Test case TC4 was used only for the determination of the flow conditions without combustion in the LDV experiments. The Reynolds number Re_H, also given in Table 2, is based on the step height H and the averaged air inlet velocity U_0 immediately above the step. For the determination of the dynamic shear viscosity, both the water content of the vitiated air and the temperature dependency were taken into account using the Wilke equation[48] and the Sutherland equation,[49] respectively.

At the beginning of every experiment at TC1, TC2 and TC3 conditions, the air heater was started to heat up the test facility and the mounted solid-fuel slab. After two minutes the slab was ignited by an additional H_2-O_2 burner mounted below the flame-holding step (see Fig. 1). The pressure inside the combustion chamber for all test runs was approximately 1 bar.

The homogeneity of the inlet airflow was determined measuring the velocity profiles with LDV directly above the flame-holding step at the $x = -5$ mm cross section with an additional TiO_2 seeding of the airflow for $\dot{m}_{air} = 0.15$ kg/s, that is, TC2. The time-averaged velocity components U and V, as well as the related rms values at this cross section, were taken at five vertical lines located between $z/H = -3.0$ and $+3.0$. Figure 4 shows the averaged velocity values of these five lines with the related rms as error bars. All values are normalized with the average value of the whole velocity field at $x/H = -0.25$, which is interpreted as the combustor inlet velocity U_0 of the airflow. The measured velocity values indicate that the flow above the step is nearly horizontal with 2% deviation for V/U_0. Only a slight increase of U/U_0 with increasing distance y from the step has been observed. These results show that the intake flowfield is sufficiently homogeneous with rms levels below 4%. The height of the boundary above the step, which influences the recirculation zone length, as shown in the literature, has been determined for this facility by Krametz and Schulte in an earlier investigation.[26] They found that for $Re_H = 4 \times 10^4$ the boundary-layerthickness is below 2 mm at the edge of the step at $x = 0$ mm.

In the case of an accelerated flow, the particle behavior within the flow has to be carefully taken into account for the evaluation of velocity measurements. Ruck,[50] for example, reports that too short recirculationzone lengths have been found in nonreacting rearward-facing step flows with large tracer particles. Particularly in solid-fuel and particle combustion processes, the effectively measured particle size distribution is larger than the original one. This is caused by agglomeration effects, condensed oxides, and also the production of larger flakes from the fuel slab. The particles sizes found in the area between the fuel slabs and the vortices show a broad distribution with its mean shifted to small diameters. Beside the small particles, bigger particles and flakes with diameters up to about 2 mm were also found. The biggest flakes were normally detected near the fuel slab and were often accompanied by many smaller ones. It is obvious that these bigger flakes are ejected from the decomposing fuel and break up into smaller ones within the flow. Quantitative results indicate

Table 2 Investigated test cases

Test case	Air mass-flow rate $\dot{m}_{air}$, kg/s	Air mass flux $\dot{g}_{air}$, kg/m^{2}s	Airflow temperature T_{air}, K	Air intake velocity u_0, m/s	Reynolds number Re_H	Mach number Ma	Stokes number St_P (0.96 μm)	Stokes number St_P (5 μm)
TC1	0.190	50.6	800	124	2.78×10^4	0.22	0.020	0.55
TC2	0.152	40.5	800	93	2.23×10^4	0.17	0.016	0.42
TC3	0.115	30.7	800	75	1.68×10^4	0.13	0.012	0.32
TC4	0.156	41.5	790	93	2.25×10^4	0.17	——	——

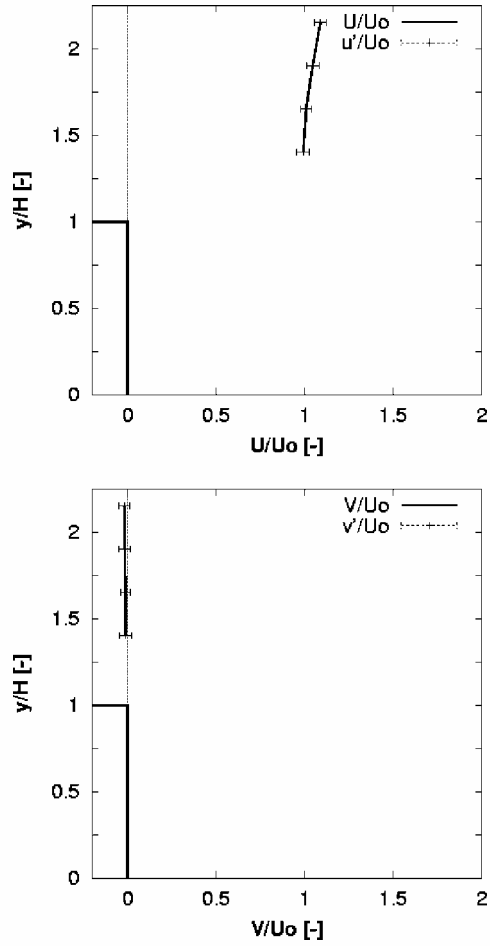

Fig. 4 Normalized entrance velocity profile at $x/H = -0.25$ ($x = -5$ mm); $U_0 = 94$ m/s; test case TC2. rms velocities (u'/U_0 and v'/U_0) are given as error bars.

large variations in the velocity and the direction of the "bigger" particles because they are too big to directly follow the gas flow. The ejection trajectories of the flakes from the fuel do not necessarily follow the streamlines of the gaseous combustion components.

A simple estimation of how particle follows the flow is given by the particle Stokes number St_P, which is defined as the ratio of the particle relaxation time $\tau_p = \rho_p d_p^2/18\eta_g$, and the fluid timescale defined as $\tau_g = H/U$. For the calculation of these quantities, the values at the air inlet flow condition have been used. Table 2 presents the Stokes number St_P for particles of the Sauter mean diameter of the original boron particles as well as the particle diameter of 5 μm of the related 10% limit. The calculated values are significantly lower than one so that most of the original particles follow the flowfield quite well. A more exact estimation of the particles flow-following behavior can be given by the solution of the Basset–Boussinesq–Oseen equation, which describes the movement of a particle in an oscillating gas. For a given amplitude and frequency of the gas-phase oscillation, the resulting amplitude and phase shift of the particle can be calculated, for example, see Refs. 35 and 50. Using the velocity and rms values of the LDV measurements presented in this publication, an estimation of the gas-phase movement has been conducted.[51] The results show that the amplitude reduction and the phase shift are beyond 1% for ideally spherical boron particles of 150 μm in the cross sections at $x/H = 4.8$ and 6.75 under TF2/TC2 conditions. For the LDV data evaluation only the data from particles of diameter less than about 50 μm were used, such that the measuring error is beyond the 1% value. Also the average velocity distribution obtained from the smallest particles in the PIV images confirm the results of the LDV measurements and are presented in this publication.

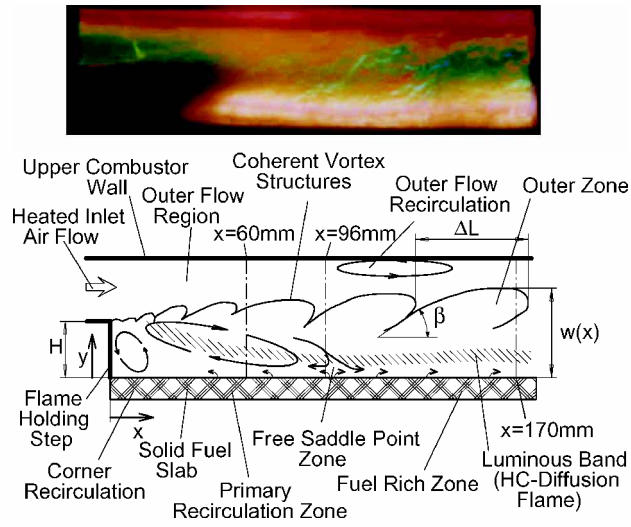

Fig. 5 Top shows a color schlieren image of HTPB without particle addition (test fuel TF1), test case TC2. Bottom shows a sketch of flowfield and combustion characteristics related to the upper image and positions of the principle measuring cross sections.

IV. Results and Discussion

A. General Features of Flowfield and Combustion Process

Figure 5 shows a color schlieren image of the combustion process of HTPB/IPDI without boron particle addition (TF1) for $\dot{m}_{\text{air}} = 0.15$ kg/s, that is, test case TC2. Below this image is a sketch of the characteristic features of the flowfield and combustion process. These features have been derived from the schlieren image above as well as from PIV images and LDV measurements. Included are also some technical terms derived from a sketch by Natan and Gany[30] regarding the combustion processes in the boundary layer of a solid-fuel ramjet. Additionally, some measured cross-section locations are presented in this sketch.

Immediately behind the rearward-facing step a separation region is located with a large clockwise-rotating recirculation zone (RZ), with an average length L_R of about five times the step height H, that is, $L_R/H \approx 5$. This has been identified by LDV measurements. At the end of this recirculation zone, the downward oriented flow from above the recirculation zone and the flow from the combustor bottom, originating from the combusting and pyrolysing solid-fuel slab, form a free saddle point.[19] For comparison with other publications, in flows without fluid feeding from the wall the end of the RZ is commonly defined as a reattachment point located at the wall.

In the lower region of the color schlieren image, a yellow glowing band can be seen, which is not visible on color schlieren images obtained with significantly shorter exposure times than the 1 ms used for the image of Fig. 5. This indicates that this band originates from thermal emissions of the condensed phase (boron, B_2O_3, TiO_2, soot, etc.) and is superimposed on the schlieren image. The thermal emissions of all test fuels investigated, TF1–TF3 (with and without particle addition), are dominated by soot. This has been shown in earlier publications,[52,53] where the spectral emissions from HTPB-based fuels and GAP-based fuels (glycidylazide polymer), both with and without boron particle addition, have been compared. As a result of the latter and in accordance with earlier investigations[30] of other researchers, this glowing band can be interpreted as the location of the hydrocarbon diffusion flame. Comparing the schlieren images obtained for TF2 (containing boron) with those of TF1, the upper border of this glowing band seems to be located somewhat higher for TF2, whereas the shape appears similar.

In the region of the free saddle point, the distance between the glowing band and the combustor bottom is smaller. This is caused by the downward-oriented movement of the flow in this region. From the left side of the schlieren image, that is, the area immediately behind the rearward-facing step, no information about the occurring processes can be obtained because of the pollution by soot and

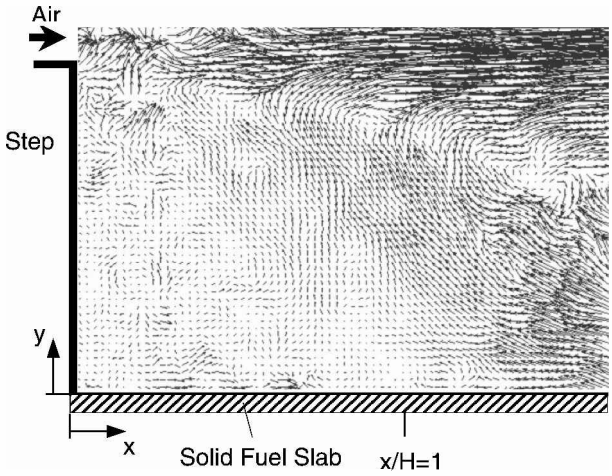

Fig. 6 Average velocity plot of the region of the secondary recirculation zone immediately behind the step, test fuel TF2, test case TC2.

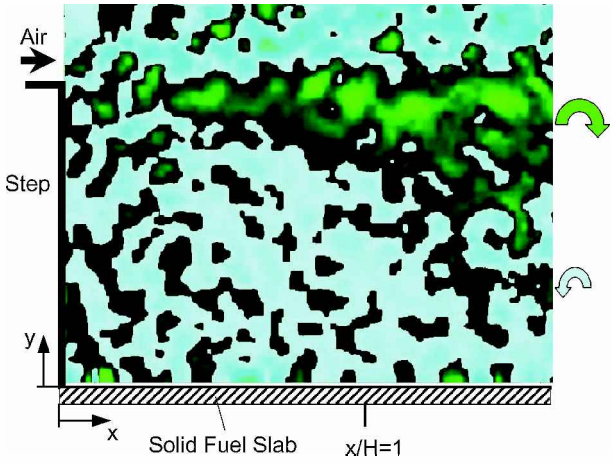

Fig. 7 Orientation and strength of rotation for TF2, TC2. The light blue color represents a counterclockwise rotation with low strength, and the green color represents clockwise rotation with a much higher strength (image averaged over approximately 20 single images).

combustion residues on the windows. Schlieren images, however, obtained with window devices with protection flow and a free inner cross section of 45×45 mm^2 show that the glowing band exists also in a large part of the lower region of the recirculation zone, and its average position is also included in the sketch of Fig. 5.

In the triangle between the upper step edge, the lower corner and a point at approximately $x/H \approx 1$ at the fuel slab surface a further but significantly smaller recirculation zone can be seen, which is well known from step flow investigations with nonreacting media. This (secondary) corner recirculation zone rotates in a direction counter to the primary recirculation zone and its strength of rotation $|\text{rot}\,\vec{v}| = \partial V/\partial x - \partial U/\partial y$ is much smaller than that of the first RZ, as can be seen on the velocity vector plot of the region immediately behind the step in Fig. 6 and the corresponding plot of the strength of rotation in Fig. 7. Figure 6 shows the velocity vectors averaged from a series of PIV images of the area immediately behind the rearward-facing step ($x = 0$ to 35 mm). In the upper-right area of the image, a part of the clockwise-rotating (primary) recirculation zone can be seen. The velocity vectors in the secondary RZ are significantly smaller than those of the primary RZ. Also, the rms values obtained at the measuring cross section at $x/H = 0.75$, which are inside this secondary RZ, show significantly lower values in comparison to the primary recirculation zone. This will be discussed in further detail in the following section. The averaged strength of rotation is presented in Fig. 7 in a false color image with three colors representing different strength value ranges. The light blue color in the lower-left part of the plot represents the left-turning rotation

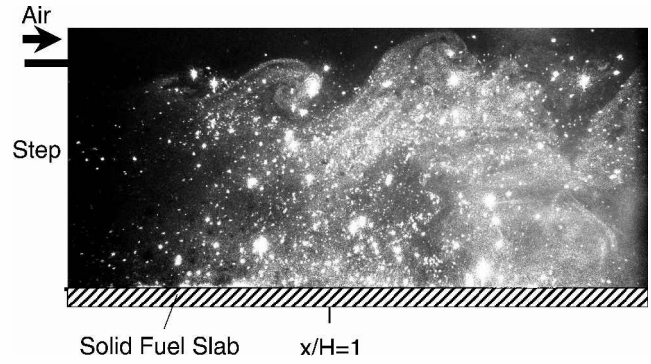

Fig. 8 Double-exposure PIV image of the area immediately behind the rearward-facing step.

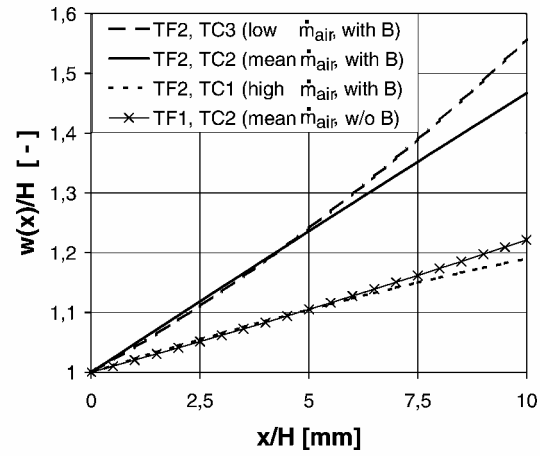

Fig. 9 Dimensionless outer border of outer zone $w(x)/H$.

in the corner RZ with low strength, and the green color represents much larger values for the right-turning rotation in the primary RZ and the developing shear layer behind the step edge.

Furthermore, large-scale coherent vortex structures can be seen on the color schlieren image of Fig. 5 in the region above the glowing band. The formation of these coherent structures is caused by an instability as a result of the turbulent state of the shear layer ($Re_H \gg 10^3$) behind the edge of the rearward-facing step as is described in the literature (e.g., see Ref. 19). In this shear layer a high rotation of the flow, which can be seen as the green color area in Fig. 7, indicates a region with intense mixing of the particles with the incoming air. This indicates that a large fraction of the particles in the outer zone of the reacting shear layer are originating from the recirculation zone. In this shear layer the vortices are growing with increasing distance x from the step until the end of the primary RZ, as can be seen in PIV images such as Fig. 8 and also color schlieren images. Hereafter the horizontal distance ΔL of the coherent vortex structures remains nearly constant. The outer border $w(x)$ of these structures, however, is still increasing in a vertical direction, as can be seen in Fig. 9. The air mass-flow variation shows that $w(x)$ increases with increasing $\dot{m}_{\text{air}}$. Also the energy release of the boron particles enlarges this region when TF2 (containing boron) is used, as compared with TF1. Figure 10 shows the dependence of ΔL on $\dot{m}_{\text{air}}$. It can be seen that ΔL increases with $\dot{m}_{\text{air}}$. It is also obvious that ΔL has the lowest values for TF1 without particle addition, so that the energy release increases the coherent vortex structures. Furthermore with increasing $\dot{m}_{\text{air}}$ the coherent structures are more stretched, and the inclination angle β decreases.

B. Velocity Distribution

To obtain sufficient data for the evaluation of the region near the outer airflow, the airflow was seeded with TiO_2 particles for some LDV experiments. The comparison of the velocities and rms values for the seeded and the unseeded cases shows no significant

Table 3 Test conditions of investigations presented in Fig. 13

Author	Reference No.	H/h	x/H	Re_H	$\dot{m}_f/\dot{m}_{air}$	ϕ	Type of flame
Pitz and Daily	23	2.0	5.0	2.2×10^4	——	0.57	Premixed flame, propane/air
Krametz and Schulte	26	2.25	5.0	4×10^4	0.0041 ($U_{CH4} = 0.06$ m/s) 0.0082 ($U_{CH4} = 0.12$ m/s)	0.07 0.14	Diffusion flame, methane feeding through porous bottom plate behind step
This work	——	2.25	4.8	2.23×10^4 (TC 2)	0.008 (TF2, TC2)	0.07	Diffusion flame, solid-fuel slab behind step

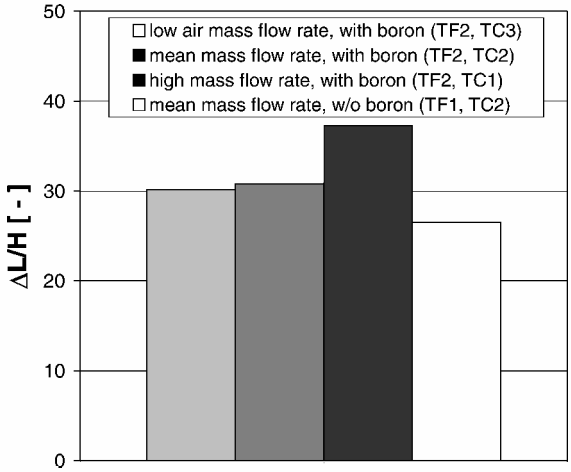

Fig. 10 Horizontal distance ΔL between coherent vortex structures.

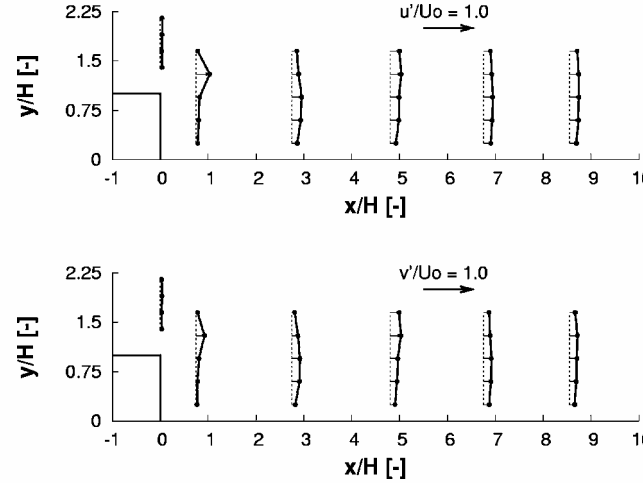

Fig. 12 Rms value plot, $z/H = 0$ mm, 30% B/HTPB/IPDI (test fuel TF2).

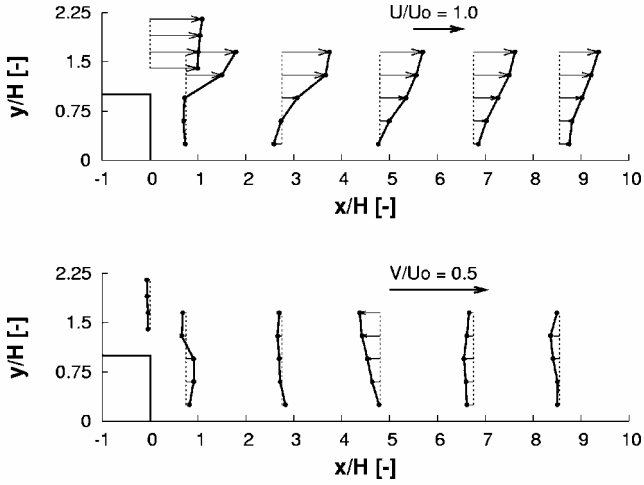

Fig. 11 Velocity vector plot, z/H = 0 mm, 30% B/HTPB/IPDI (test fuel TF2).

differences, as can be seen in Ref. 43. This also indicates that the majority of the boron particles, which were used for the LDV velocity determination, follow the flowfield quite well.

Figure 11 presents the time-averaged velocity components U and V of several measured cross-section locations for test case TC2. The data of the traces have been averaged arithmetically from the three measuring locations $z/H = -1.5$, 0, $+1.5$ in this plane. Because the burning solid-fuel slab reaches only from $-2.5 < z/H < 2.5$, the data obtained at $z/H = +3.0$ and -3.0 were measured above the metallic base plate and are not included. Considering all of the data in the measuring planes, which are not presented here, relatively good two-dimensional flow characteristics can be seen downstream from the recirculation zone, whereas only the V-rms at the outer borders at $z/H = +3$ and -3 has lower values. All U velocity traces in Fig. 11 show increasing values up to the value of the outer airflow above the combustion zone. The U traces behind the step show negative values up to $x/H = 4.8$ indicating the primary recirculation zone with its downstream end at about five times the step height. The related V velocity component shows the clockwise rotation in this region, whereas the strongest negative values exist at $x/H = 4.8$. Downstream of this plane, the flow in the reacting boundary layer is oriented more horizontally, and there is an acceleration in the streamwise direction.

Figure 12 shows the rms values for U and V corresponding to the velocity distributions of the measuring cross sections presented in Fig. 11. The lowest values for both rms were found in the first measured cross-section location behind the step, where the small corner recirculation zone is located. The highest values of each cross section were measured near the middle of the chamber, where the shear layer with the embedded coherent vortex structures is present. Summarizing both U- and V-rms values, a small maximum occurs near the upper combustor wall in the outer airflow at the measured cross-section location at $x/H = 4.8$. This indicates a further small recirculation zone, which is the vortex corresponding to the large recirculation zone. The existence of such a recirculation zone in the outer airflow has also been described in the literature regarding cold-flow investigations. This outer-flow recirculation was included in the sketch of the characteristic features of the flowfield and combustion in Fig. 5.

In Fig. 13 the velocity and rms values near the cross section $x/H = 5$ for TC4 flow conditions without combustion and for test fuels TF1, TF2, and TF3 under test-case TC2 conditions are presented together with data from the literature. The test conditions of all related experiments are listed in Table 3. The data of TC2 and TC4 used in Fig. 13 have also been averaged arithmetically in this measuring plane from the three measuring locations $z/H = -1.5$, 0, $+1.5$, and are presented as solid lines. Pitz and Daily[23] investigated the combustion of a premixed propane/air mixture under nearly the same Re_H conditions but with a slightly higher expansion ratio $h/(h - H)$ than in the experiments of this publication. Also the equivalence ratio ϕ of their reacting flow case is eight times higher than for TF2 at TC2 condition. Krametz and Schulte[26] used the same test facility as described in this publication and investigated the combustion behavior of methane, which was fed through

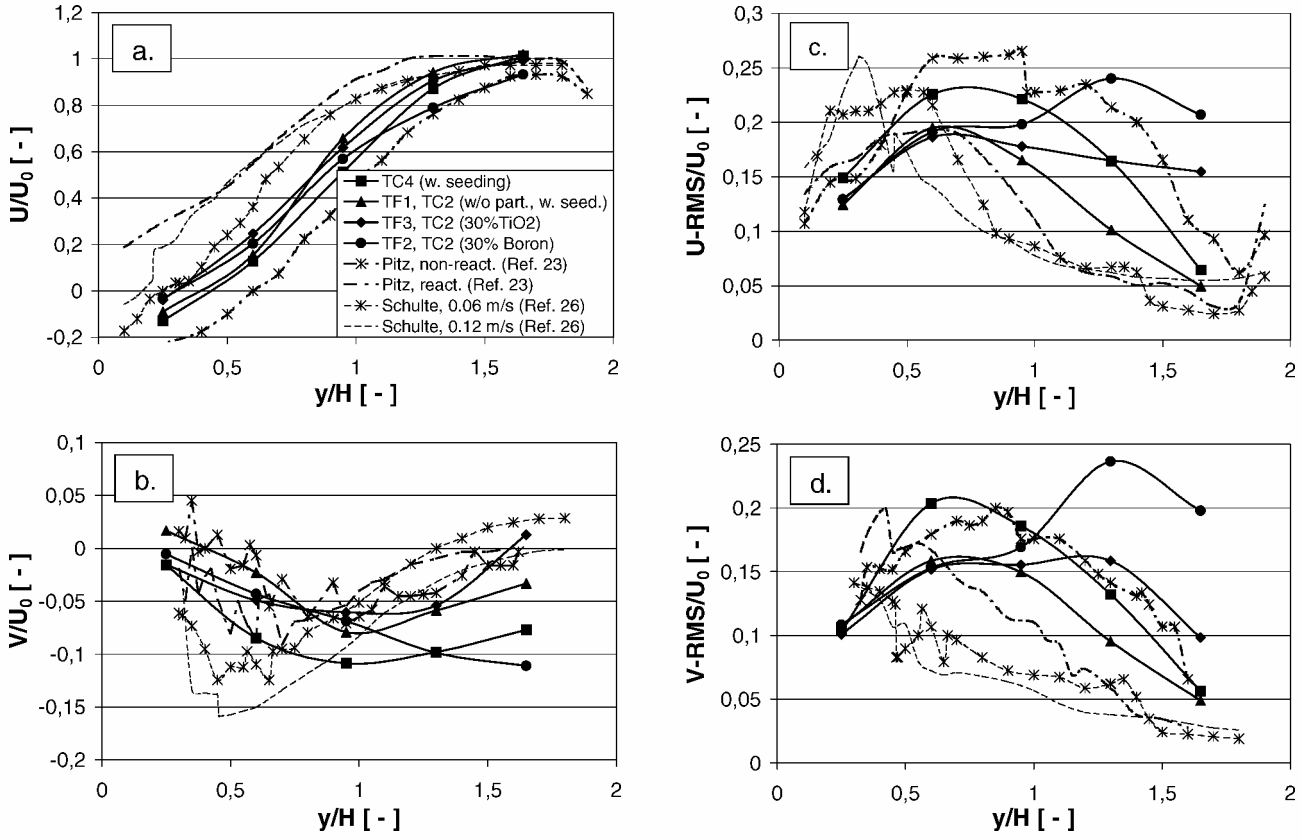

Fig. 13 Comparison of velocity components and rms values near the cross section at $x/H = 5.0$.

a porous plate behind the step in order to simulate a pyrolysing solid-fuel slab. The Re_H of their investigations is as twice as high, and the air inlet temperature is significantly lower than in TC2.

The shapes of all U-velocity component traces in Fig. 13a are similar and show increasing values with increasing distance y up to around $y/H = 1.6$ (except Pitz). In the outer flow region above $y/H = 1.6$ the velocity remains constant. The lower values of Pitz and Daily's nonreacting test case can be explained by the higher expansion ratio in their experimental device. Also the decrease above $y/H = 1.8$ is caused by the boundary layer at the upper combustor wall in the smaller combustion chamber. The results of test cases TC2 and TC4 show negative velocity values near the combustor base, indicating backflow near the end of the recirculation zone. Comparing the traces of the three combustion experiments at TC2 with the nonreacting flow TC4, the negative velocity values are reduced, indicating a reduction of the recirculation zone length L_R as a result of the energy release in the flowfield. Also the velocity values of TF2 (containing boron) are significantly lower than the other traces at TC2 conditions above $y/H = 1.0$, indicating a shift of the outer border of the outer zone $w(x)$, as can also be seen in the schlieren images, as is presented in Fig. 9. The reduction of L_R can also be seen if the traces for the reacting and the nonreacting cases of Pitz and Daily are compared. Here the reduction is more pronounced because of the significantly higher energy release mainly above and behind the recirculation zone at the higher ϕ. Comparing the results of TF2 (containing boron) at TC2 with the results of Krametz and Schulte at the methane feeding velocity $U_{CH4} = 0.06$ m/s and at the same equivalence ratio $\phi = 0.07$, slightly shorter L_R occurs for the methane combustion. Also higher U velocities were observed at higher y/H for the CH_4 combustion process. Taking the V-velocity components also into account, a more distinct downward movement of the flow can be seen, occuring immediately behind the end of the primary recirculation zone. The reduction of L_R can also be seen in Schulte's experiment with the doubling of the methane feeding velocity U_{CH4} and the equivalence ratio ϕ.

The V-velocity component is presented in Fig. 13b. The nonreacting flow TC4 shows negative values with a minimum near $y/H = 1$, indicating the downward movement of the flow behind the primary recirculation zone. Except in the case of TF2-containing boron, the reacting flows at TC2 show higher values, indicating both the reduction of L_R and an increase in volume in the reacting shear layer caused by energy release. TF2 shows values similar to those of TF3 (containing TiO_2) below $y/H = 1$. Above $y/H = 1$ a further decrease with increasing y also indicates the shift of $w(x)$ as a result of the energy release of the reacting boron particles at higher y. The results of Krametz and Schulte have significantly lower V velocities beyond $y/H = 0.7$ and a shift of the minimum to $y/H \approx 0.5$ in comparison to our experiments (except with boron) as has been mentioned earlier. This can be caused by a stronger downward movement behind the shorter recirculation zone. The nonreacting trace of Pitz and Daily is similar to TC4, but is shifted to higher values and is less smooth. The V component of their reacting case is lower than their nonreacting trace beyond $y/H = 1$ and higher above $y/H = 1$ because in this premixed flow the reaction zone is located at about $y/H = 1$.

The rms values of the nonreacting flow of TC4 presented in Figs. 13c and 13d are similar to those of Pitz and Daily and show broad maxima around $y/H = 0.7$. Both U- and V-rms traces of TF1 without particle addition are lower than the traces of the nonreacting flow TC4, which is typical for reacting flows. The traces of the particle-containing fuels TF2 and TF3 show values similar to those of TF1 below around $y/H = 1.0$. Above $y/H = 1.0$ they have significantly higher U- and V-rms values. This can be related to the movement of the particles within the coherent vortex structures in this area, which can be seen in color schlieren as well as the PIV images. The stronger increase for test fuel TF2 seems to be caused by the combustion of the boron particles and the higher energy release because the addition of combustible boron particles is the only condition that is changed. The results of Krametz and Schulte show distinct maxima for U-rms below $y/H = 0.6$ with significantly higher values in this area than at the maxima of our results and significantly lower values at higher y/H. This might be explained by more complete combustion in Schulte's experiment at the same equivalence ratio in comparison to our experiment, where

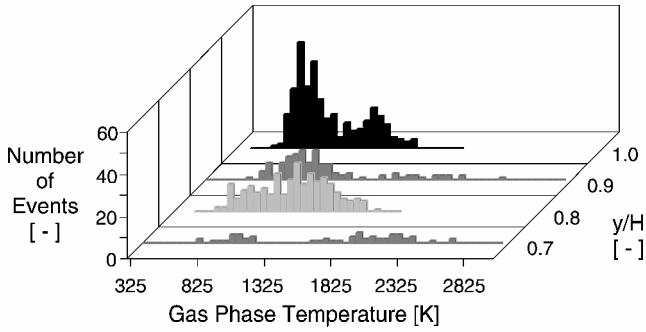

Fig. 14 Temperature histograms of TF2 (30% B/HTPB/IPDI) at different heights y/H above the combustor bottom at $x/H = 8.5$ ($x = 170$ mm), $z/H = 0$, test case TC2.

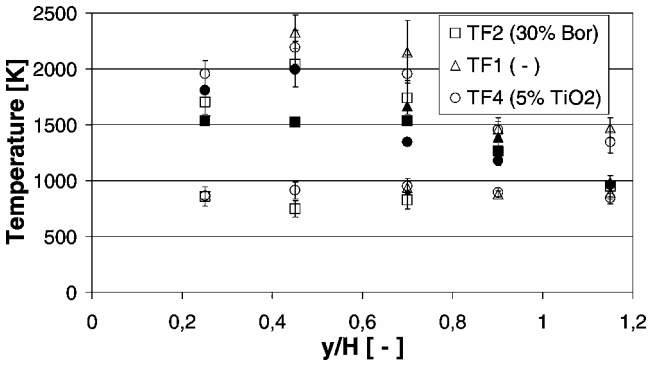

Fig. 15 Temperature distribution of three different test fuels at $x/H = 14.5$ ($x = 290$ mm), TC2.

the reaction zone in the multiphase combustion of the *HC*-solid-fuel slab with the embedded particle phase is broader.

C. Temperature and Concentration Distribution

The intense mixing process can also be identified on the gas-phase temperature histograms obtained with CARS. Each bar of 50-K width in the diagram in Fig. 14 presents the number of fitted temperatures to obtained spectra recorded at 10 Hz during a test run. In the histogram for $y/H = 1$ ($y = 20$ mm), a bimodal temperature distribution with two distinct maxima can be seen. The left maximum has an average temperature of about 850 K and can be related to the temperature of the outer airflow. At higher temperatures a broad maximum can be seen with an average temperature of about 1750 K. This bimodal distribution is caused by the movement of "colder" air to lower regions by the coherent vortex structures as can be seen in both the color schlieren and PIV images. Under the assumption that the small particles follow the gas flow quite well, the areas with high particle number density in the vortices on Fig. 8 seem to be significantly hotter. At lower y the bimodal behavior is strongly reduced, and the average temperature increases with decreasing y. Below $y/H = 0.7$ (14 mm) the success of the spectra evaluation was very low because of C_2 interferences, etc., and so the number of events is too low to present meaningful histograms.

Figure 15 shows the averaged gas-phase temperatures for three different test fuels at the measured cross-section location at $x/H = 14.5$ ($x = 290$ mm). The open symbols represent the mean temperatures for each of the bimodal distributions and the solid symbols the averaged temperature for the whole histogram. The standard deviations are also included in this diagram. At this measured cross-section location, located downstream of the burning slab, sufficient data could even be obtained near the lower wall. This is caused both by the advanced consumption of the combustion intermediate reaction products and the advanced dilution with the outer airflow through the coherent vortex structures. This hypothesis is supported by the slightly bimodal temperature distributions obtained even at $y/H = 0.25$ (5 mm). The highest temperatures for the upper

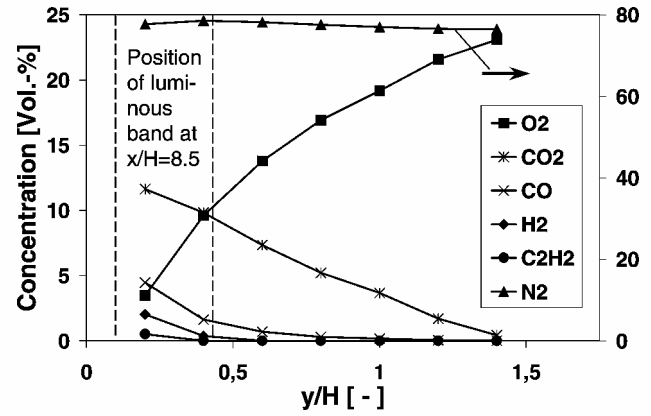

Fig. 16 Concentrations of gaseous stable (intermediate) reaction products vs the vertical distance y/H from the combustion chamber bottom at $x/H = 8.5$ ($x = 171$ mm), $z/H = 0$, TF2, test case TC2.

maxima as well as the overall average temperatures were obtained at $y/H = 0.45$ (9 mm) while at $y/H = 1.15$ (23 mm) the overall average temperatures are near T_{air} with only a few incidents of higher temperatures. At $y/H = 0.4$ and 0.7 the fuel TF1 without particle addition shows the highest temperatures. Because both TiO_2 (5 wt-%) and boron particles (30 wt-%) act as a heat sink at lower y and the energy release of boron is relatively low in this region, this behavior can be explained. At $y/H = 0.7$ and above TF2 (containing boron) shows slightly higher overall average temperatures, which can be explained by a further consumption of boron in this region.

Figure 16 shows concentration profiles as volume ratios X_i of the gaseous (intermediate) reaction products, which were collected in the sampling cylinders and which are stable at ambient temperatures. The measuring cross section was located at $x/H = 8.5$ ($x = 171$ mm) in the reacting boundary layer behind the primary recirculation zone. The diagram shows profiles with decreasing values for CO_2, CO, H_2, and C_2H_2 with increasing distance y from the combustion chamber base, while the oxygen concentration increases as a function of the same parameter y up to the border of the outer airflow. Also methane and C_2H_4 were found with values below 0.2% at $y/H = 0.2$. The position of the luminous band is included in this diagram. It can be seen that the hydrogen is depleted above the upper border of this band and that the concentration of hydrocarbons is below the detection level of the gas-chromatograph.

The concentration profiles of the main species O_2, CO, and CO_2, which were obtained at four cross-section locations between $x/H = 3$ ($x = 60$ mm) and $x/H = 14.6$ ($x = 292$ mm), are presented in Figs. 17a–17c in separate diagrams. The oxygen content increases for all traces with increasing y. With increasing distance x from the rearward-facing step, the O_2 content increases for all vertical positions y, with the exception of the region above $y/H \approx 0.5$ for $x/H = 14.6$. The O_2 trace shows significantly lower values in the region of the primary recirculation zone at $x/H = 3$ with only a slight increase below $y/H = 0.8$ in comparison to the trace from the developing reacting boundary layer behind the recirculation zone at $x/H = 8.5$. Above $y/H = 0.8$ a more distinct increase can be seen as a result of the intense mixing by the coherent vortex structures in the shear layer above the recirculation zone. The CO_2 trace in Fig. 17c shows for this cross section beyond $y/H = 0.8$ nearly constant values and above a steep decrease. Only the corresponding CO values show a continuous decrease for the whole trace with significantly higher values than for all other cross sections, indicating the conversion of CO to CO_2 in this region.

At the measured cross-section location near the end of the recirculation zone at $x/H = 4.8$, the concentration curves show a tendency similar to that of the traces at $x/H = 8.5$, whereas lower O_2 and higher CO and CO_2 values have been found. The CO remains nearly constant only between $y/H = 0.6$ and 1.0, and it decreases thereafter quickly to 0, which is at $y/H = 1.2$ the lowest value in all cross sections. This CO irregularity is combined with slight irregularities in the slopes of O_2 and CO_2. This is caused both by the

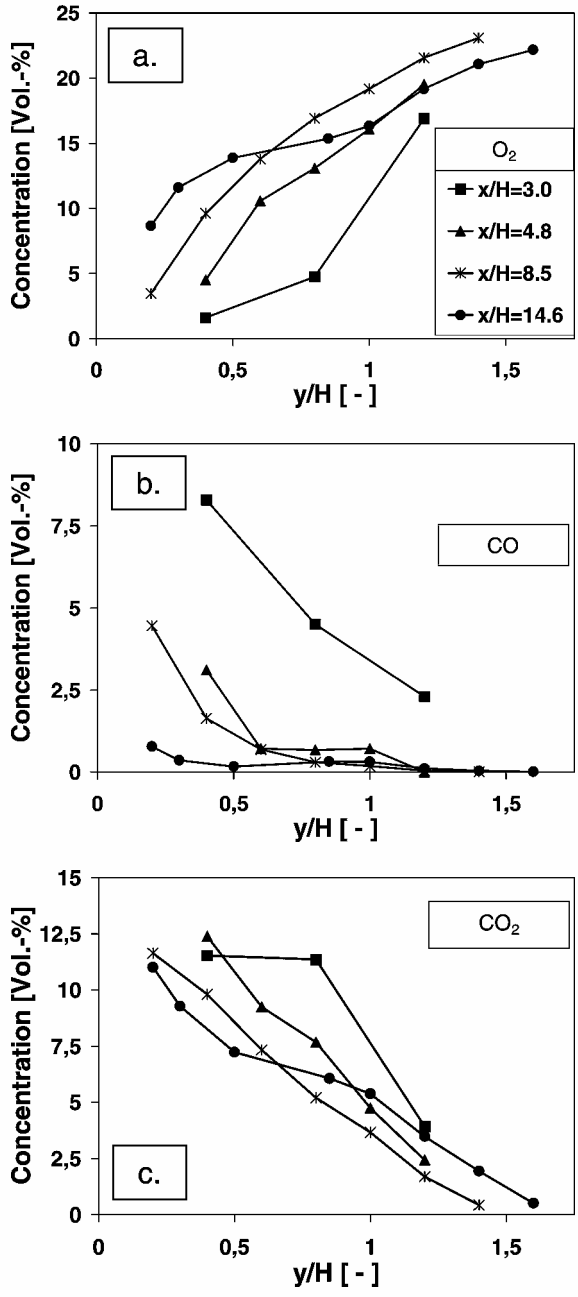

Fig. 17 Concentration profiles X_i of O_2, CO and CO_2 vs the vertical distance y/H from the combustion chamber bottom for various cross sections, $z/H = 0$, TF2, TC2.

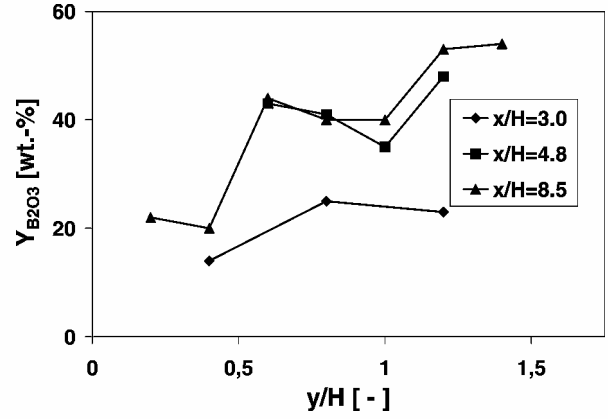

Fig. 18 Boron-oxide content Y_{B2O3} of the collected solid phase vs y/H for three measuring cross sections, $z/H = 0$, TF2, TC2.

stronger downward movement of the flow in this region behind the recirculation zone and by the intense mixing process with very high rms values in this region, as can be seen in Fig. 12. At the cross section $x/H = 14.6$, which is located downstream of the end of the fuel slab at $x/H = 10$, these irregularities can also be seen. Especially for the traces of O_2 and CO_2, they are much more pronounced and indicate an intense mixing process with the outer airflow and possibly a further recirculation zone behind the end of the solid-fuel slab at $x/H = 10$. This might be caused by the flow over the upward step formed as a result of the regression of the fuel slab (which is embedded in the combustor base) by the combustion process.

Figure 18 shows the boron-oxide content Y_{B2O3} in the solid phase (at ambient temperature), which was collected on the filter, against the vertical position y for three different cross sections at $x/H = 3$, 4.8 and 8.5. At the measuring cross section at $x/H = 3$, located near the center of the primary recirculation zone, the curve shows significantly lower values than those from the other cross sections and a slight maximum below $y/H = 1.0$. At the other two cross sections behind the primary recirculation zone, the B_2O_3 content shows an upward tendency with increasing distance y from the combustor bottom with an embedded small minimum near $x/H = 1.0$. Despite the estimated comparatively large relative measurement error of around 20%, the tendency in both traces is similar. In general, the upward tendency indicates a higher conversion ratio of the boron particles to boron oxide with increasing distance y from the combustor bottom and increasing distance from the rearward-facing step. The minimum with the subsequent second increase can be explained by the fact that boron particles originating from the primary recirculation zone are extracted by the coherent vortex structures in the shear layer above and are moved downstream in this outer zone. Because of the combustion of these boron particles in the hot particle-rich layers of the coherent vortex structures, the boron-oxide content increases again. This is supported also by the CARS measurements at $x/H = 8.5$, where even at the higher position $y = 20$ mm a bimodal temperature distribution exists with an average upper maximum temperature of 1750 K, as can be seen in Fig. 14. Above $y/H = 1.4$ the sampling probe was not used, and so information about the boron-oxide content could not be determined.

V. Conclusions

The combustion behavior of solid-fuel slabs containing boron particles has been investigated in a planar step combustor under conditions of air inlet temperature and velocity relevant to ramjet applications. The main characteristics of the flowfield have been determined using various intrusive and nonintrusive diagnostic techniques. Large-scale coherent vortex structures have been observed in the outer zone above the diffusion flame, which is embedded in the developing boundary layer behind the recirculation zone. These vortices are produced in the shear layer above the primary recirculation zone and grow in size up to the area of the free saddle point. Downstream of that point the streamwise distance of the vortices remains nearly constant, with the border of the outer zone still increasing. Gas-phase temperature measurements with CARS show bimodal gas-phase temperature distributions in this zone with the coherent vortex structures. Further smaller counter-rotating recirculation zones have been observed in the lower corner immediately behind the step (below the clockwise-rotating primary recirculation zone) and at the upper combustor wall behind the end of the primary recirculation zone.

The velocity diagrams show a reduction of the primary recirculation zone length as a result of the energy release with combustion in comparison to the nonreacting flow case. The U- and V-rms values of the test cases without particle additives to the solid fuel show maxima at around $y/H = 0.8$ at the measured cross-section location near the end of the primary recirculation zone. The reacting cases with the particle-containing fuels, however, show in this cross section significantly higher values above $y/H = 1$, whereas for the boron-containing fuel a distinct maximum occurs at around $y/H = 1.3$.

The distribution of stable gaseous (intermediate) reaction products behind the primary recirculation zone is similar to a diffusion flame in a developing boundary layer. O_2 increases with increasing distance continuously from the combustor base at all measuring cross sections, while CO, CO_2, and hydrocarbons are decreasing. The boron-oxide content of the collected solid phase shows an upward tendency with increasing distance from the combustor base. The boron-oxide content also increases with increasing distance from the rearward-facing step. The locations of the reaction zones of the hydrocarbons and the boron particles are different. The hydrocarbons are mainly consumed up to around $y/H = 0.5$ as can be seen by a distinct luminous (yellow glowing) band on color schlieren images. The boron combustion zone, however, is much broader, whereas above the luminous band the consumption occurs in the hot particle-laden layers in the coherent vortex structures.

The distributions of the gaseous species as well as the boron-oxide content of the collected solid phase show a discontinuity in the cross section near the end of the primary recirculation zone at about $y/H = 1$, which also can be explained by the intense mixing and combustion process in this region. The embedded slight minimum in the B_2O_3 trace and the subsequent increase can be related to the combustion of boron particles originating from the primary recirculation zone. They are extracted from this zone by the coherent vortex structures in the shear layer between the outer airflow and the recirculation zone.

Acknowledgments

The authors wish to thank their colleagues, who contributed to this paper: S. Anders and R. Brändle for chemical analysis of the gas and particle sampling probes, J. Liebl for the production of the solid-fuel slabs, and D. Heiler for the manufacture of the sampling probes.

References

[1]Gany, A., "Combustion of Boron-Containing Fuels in Solid Fuel Ramjets," *Combustion of Boron-Based Solid Propellants and Solid Fuels*, edited by K. K. Kuo and R. Pein, CRC Press, Boca Raton, FL, 1993, pp. 91–112.

[2]King, M. K., "A Review of Studies of Boron Ignition and Combustion Phenomena at Atlantic Research Corporation over the Past Decade," *Combustion of Boron-Based Solid Propellants and Solid Fuels*, edited by K. K. Kuo and R. Pein, CRC Press, Boca Raton, FL, 1993, pp. 1–80.

[3]Chase, M. W., Davies, C. A., Downey, J. R., Frurip, D. J., McDonald, R. A., and Syverud, A. N., "JANAF Thermochemical Tables," *Journal of Physical and Chemical Reference Data*, Vol. 14, Suppl. No. 1, 1985, pp. 175, 269.

[4]Meinköhn, D., "Oxide Layer Effects in Metal Particle Combustion," *Proceedings of the 5th International Microgravity Combustion Workshop*, NASA CP-1999-208917, NASA Glenn Research Center, Cleveland, edited by K. Sacksteder, 1999, pp. 219–222.

[5]Faeth, G. M., "Status of Boron Combustion Research," *21st JANNAF Combustion Meeting*, CPIA Publications 412, Vol. 2, 1984, pp. 15–29.

[6]Macek, A., "Combustion of Boron Particles: Experiment and Theory," *Proceedings of 14th (International) Symposium on Combustion*, Combustion Inst., Pittsburgh, PA, 1972, pp. 1401–1411.

[7]Yeh, C. L., and Kuo, K. K., "Ignition and Combustion of Boron Particles," *Progress in Energy and Combustion Sciences*, Vol. 22, 1996, pp. 511–541.

[8]Kaskan, W. E., and Millikan, R. C., "Spectroscopic Studies of Flame Gases Containing Boron," *Proceedings of 8th (International) Symposium on Combustion*, Combustion Inst., Pittsburgh, PA, 1962, pp. 262–275.

[9]Morrison, M. E., and Scheller, K., "Spectral Characteristics of Hydrocarbon-Air Flames Containing Aluminium, Magnesium and Boron," *Combustion and Flame*, Vol. 13, Feb. 1969, pp. 93–97.

[10]Li, S. C., Williams, F. A., and Takahashi, F., "An Investigation of Combustion of Boron Suspensions," *Proceedings of 22nd (International) Symposium on Combustion*, Combustion Inst., Pittsburgh, PA, 1988, pp. 1951–1960.

[11]Clauß, W., "Verbrennung von Borstaubwolken in Wasserdampfhaltigem Heißgas," DLR, Internal Rept., IB 643-88/6, Lampoldshausen, Germany, April 1988.

[12]Ulas, A., Kuo, K. K., and Gotzmer, C., "Effects of Fluorine-Containing Species on the Ignition and Combustion of Boron Particles: Experiment and Theory," *Combustion of Energetic Materials*, edited by K. K. Kuo and L. DeLuca, Begell House, Inc., New York, 2002, pp. 453–463.

[13]Rood, T. J., Spalding, M. J., Krier, H., and Burton, R. L., "Ignition Dynamics of Boron Particles in a Shock Tube," AIAA Paper 97-3234, July 1997.

[14]Foelsche, R. O., Burton, R. L., and Krier, H., "Boron Particle Ignition and Combustion at 30–150 atm," *Combustion and Flame*, Vol. 117, No. 1/2, 1999, pp. 32–58.

[15]Pace, K. K., Jarymowycz, T. A., Yang, V., and Kuo, K. K., "Effect of Magnesium-Coated Boron Particles on Burning Characteristics of Solid Fuels in High-Speed Crossflows," *Combustion of Boron-Based Solid Propellants and Solid Fuels*, edited by K. K. Kuo and R. Pein, CRC Press, Boca Raton, FL, 1993, pp. 332–347.

[16]Eaton, J. K., and Johnston, J. P., "A Review of Research on Subsonic Turbulent Flow Reattachment," *AIAA Journal*, Vol. 19, No. 9, 1981, pp. 1093–1100.

[17]Nezu, I., and Nakagawa, H., "Turbulent Structure of Backward-Facing Step Flow and Coherent Vortex Shedding from Reattachment in Open-Channel Flows," *Turbulent Shear Flows 6*, Springer-Verlag, Berlin, 1989, pp. 313–337.

[18]Herzberg, J. R., and Ho, C. M., "Time-Averaged, Three-Dimensional Flow in a Rectangular Sudden Expansion," *AIAA Journal*, Vol. 30, No. 10, 1992, pp. 2420–2425.

[19]Leder, A., *Abgelöste Strömungen: Physikalische Grundlagen*, Vieweg, Braunschweig, Germany, 1992.

[20]Keller, J. O., Vanefeld, L., Korschelt, D., Hubbard, G. L., Ghoniem, A. F., Daily, J. W., and Oppenheim, A. K., "Mechanism of Instabilities in Turbulent Combustion Leading to Flashback," *AIAA Journal*, Vol. 20, No. 2, 1982, pp. 254–262.

[21]Gould, R. D., Stevenson, W. H., and Thompson, H. D., "The Turbulence Characteristics of a Separated Flow with Combustion," *Proceedings of 4th Symposium on Applications of Laser Anemometry to Fluid Mechanics, Lisbon*, 1988, pp. 4.6.1–4.6.6.

[22]Gould, R. D., Stevenson, W. H., and Thompson, H. D., "Simultaneous Velocity and Temperature Measurements in a Premixed Dump Combustor," *Journal of Propulsion and Power*, Vol. 10, No. 5, 1994, pp. 639–645.

[23]Pitz, R. W., and Daily, J. W., "Combustion in a Turbulent Mixing Layer Formed at a Rearward-Facing Step," *AIAA Journal*, Vol. 21, No. 11, 1983, pp. 1565–1570.

[24]Gabruk, R. S., and Roe, L. A., "Velocity Characteristics of Reacting and Nonreacting Flows in a Dump Combustor," *Journal of Propulsion and Power*, Vol. 10, No. 2, 1994, pp. 148–154.

[25]Schadow, K. C., Cordes, H. F., and Chieze, D. J., "Experimental Studies of Combustion Processes in a Tubular Combustor with Fuel Addition Along the Wall," *Combustion Science and Technology*, Vol. 19, 1978, pp. 51–57.

[26]Krametz, E., and Schulte, G., "The Influence of Different Fuel/Air Ratios on the Reacting Flow Field Behind a Rearward Facing Step," *Proceedings of 3rd International Conference of Laser Anemometry—Advances and Applications*, University of Manchester, GB, edited by J. T. Turner, 1989.

[27]Tsau, F. H., and Strahle, W. C., "Prediction of Turbulent Combustion Flowfields Behind a Backward-Facing Step," *Journal of Propulsion and Power*, Vol. 6, No. 3, 1990, pp. 227–236.

[28]Gany, A., and Netzer, D. W., "Combustion Studies of Metallized Fuels for Solid Fuel Ramjets," AIAA Paper 85-1177, July 1985.

[29]Jarymowycz, T. A., Yang, V., and Kuo, K. K., "Analysis of Boron Particle Ignition Above a Burning Solid Fuel in a High-Velocity Environment," *Combustion of Boron-Based Solid Propellants and Solid Fuels*, edited by K. K. Kuo and R. Pein, CRC Press, Boca Raton, FL, 1993, pp. 303–331.

[30]Natan, B., and Gany, A., "Ignition and Combustion of Boron Particles in the Flowfield of a Solid Fuel Ramjet," *Journal of Propulsion and Power*, Vol. 7, No. 1, 1991, pp. 37–43.

[31]Ciezki, H. K., Clauß, W., Feinauer, A., Sender, J., and Thumann, A., "Investigation of the Combustion Process of Boron Particle Containing Solid Fuel Slabs in a Rearward Facing Step Combustor," AIAA Paper 2000-3347, July 2000.

[32]Cords, P. H., "A High Resolution, High Sensitivity Colour Schlieren Method," *SPIE Journal*, Vol. 6, No. 3, 1968, pp. 85–88.

[33]Ciezki, H., "Entwicklung eines Farbschlierenverfahrens unter besonderer Berücksichtigung des Einsatzes an einem Stoßwellenrohr," M.S. Thesis, Technical Univ. Aachen, Institut für Allgemeine Mechanik, Germany, Jan. 1985.

[34]Ciezki, H. K., "Investigation of the Combustion Behaviour of Solid Fuel Slabs in a Planar Step Combustor with a Colour Schlieren Technique," AIAA Paper 99-2813, June 1999.

[35]Ciezki, H. K., and Sender, J., "Experiences with Various Diagnostic Techniques for the Investigation of the Multiphase Combustion Process of Energetic Particle Containing Solid Fuels with Regard to Ramjet Relevant Conditions," *Energetic Materials*, edited by U. Teipel (to be published).

[36]Adrian, R. J., "Statistical Properties of Particle Image Velocimetry Measurements in Turbulent Flow," *Laser Anemometry in Fluid Mechanics*, Vol. III, Ladoan-Inst., Tecnico, Lisbona, Portugal, 1988, pp. 115–129.

[37]Grant, I., and Smith, G. H., "Modern Developments in Particle Image Velocimetry," *Optics and Lasers in Engineering*, Vol. 9, Nos. 3–4, 1988, pp. 245–264.

[38] Adrian, R. J., "Particle-Imaging Techniques for Experimental Fluid Mechanics," *Annual Review of Fluid Mechanics*, Vol. 23, 1991, pp. 261–304.

[39] Thumann, A., and Ciezki, H. K., "Comparison of PIV and Colour-Schlieren Measurements of the Combustion Process of Boron Particle Containing Solid Fuel Slabs in a Rearward Facing Step Combustor," *Combustion of Energetic Materials*, edited by K. K. Kuo and L. DeLuca, Begell House, Inc., New York, 2002, pp. 742–752.

[40] Raffel, M., Willert, C., and Kompenhans, J., *Particle Image Velocimetry*, Springer-Verlag, Berlin, 1998.

[41] Yamamoto, F., Uemura, T., Koukawa, M., Itoh, M., and Teranishi, A., "Application of Flow Visualisation and Digital Image Processing Techniques to Unsteady Viscous Diffusing Free Doublet Flow," *Proceedings of 2nd International Symposium on Fluid-Control, Measurement, Mechanics and Flow Visualization*, 1988, pp. 184–188.

[42] Jambunathan, K., Ju, X. Y., Dobbins, B. N., and Ashforth-Frost, S., "An Improved Cross Correlation Technique for Particle Image Velocimetry," *Measurement Science and Technology*, Vol. 6, No. 5, 1995, pp. 507–514.

[43] Sender, J., and Ciezki, H. K., "Velocities of Reacting Boron Particles Within a Solid Fuel Ramjet Combustion Chamber," *Defence Science Journal*, Vol. 48, No. 4, 1998, pp. 343–349.

[44] Clauß, W., Vereschagin, K., and Ciezki, H. K., "Determination of Temperature Distributions by CARS-Thermometry in a Planar Solid Fuel Ramjet Combustion Chamber," AIAA Paper 98-0160, Jan. 1998.

[45] Ciezki, H. K., Clauß, W., Thumann, A., and Vereschagin, K., "Untersuchung zur Temperaturverteilung mittels CARS-Thermometrie in einer Modell-Staubrennkammer beim Abbrand von Festbrennstoffplatten," *Proceedings of 30th International Annual Conference of ICT*, edited by G. Langer, Fraunhofer-Institut für Chemische Technologie, Pfinztal, Germany, 1999, pp. 31.1–31.15.

[46] Ciezki, H. K., "Determination of Concentration Distributions of Gaseous and Solid Intermediate Reaction Products in a Combustion Chamber by a Water Cooled Sampling Probe," *Proceedings of Sensor 99, 9th International Trade Fair and Conference for Sensors, Transducers and Systems*, AMA Service GmbH, Wunstorf, Germany, Vol. 1, 1999, pp. 327–332.

[47] Ciezki, H. K., and Schwein, B., "Investigation of Gaseous and Solid Reaction Products in a Step Combustor Using a Water-Cooled Sampling Probe," AIAA Paper 96-2768, July 1996.

[48] Bird, R. B., Stewart, W. E., and Lightfood, E. N., *Transport Phenomena*, Wiley, New York, 1960, p. 24.

[49] Truckenbrodt, E., *Fluidmechanik*, 3rd ed., Vol. 1, Springer-Verlag, Berlin, 1989, p. 14.

[50] Ruck, B. (ed.), *Lasermethoden in der Strömungsmechanik*, AT-Fachverlag, Stuttgart, Germany, 1990, pp. 130–138.

[51] Bobay, L., "Behavior of Particle Additives in the Turbulent Environment of a Solid Fuel Ramjet Combustion Chamber," DLR, Internal Rept. DLR/IB 647-2002/08, Lampoldshausen, Germany, Aug. 2002.

[52] Ciezki, H. K., Hensel, C., and Liehmann, W., "Spectroscopic Investigation of the Combustion Behaviour of Boron Containing Solid Fuels in a Planar Step Combustor," *Proceedings of 13th International Symposium on Airbreathing Engines (ISABE)*, edited by F. S. Billig, AIAA, Reston, VA, USA, Vol. 1, 1997, pp. 582–590.

[53] Blanc, A., Ciezki, H. K., Feinauer, A., and Liehmann, W., "Investigation of the Combustion Behaviour of Solid Fuels with Various Contents of Metal Particles in a Planar Step Combustor by IR-Spectroscopic Methods," AIAA Paper 97-3233, July 1997.